A study on some basic features of inertial oscillations and near-inertial internal waves

Shengli Chen, Daoyi Chen, Jiuxing Xing

Shenzhen Key Laboratory for Coastal Ocean Dynamic and Environment, Graduate School at Shenzhen, Tsinghua University, Shenzhen 518055, China.

Correspondence to: Jiuxing Xing (jxx2012@sz.tsinghua.edu.cn)

Abstract

Some basic features of inertial oscillations and near-inertial internal waves are investigated by simulating a two-dimensional (x-z) rectangular basin (300 km $\times$60 m) driven by a wind pulse. For the homogeneous case, near-inertial motions are pure inertial oscillations. The inertial oscillation shows typical opposite currents between surface and lower layers, which is formed by the feedback between barotropic waves and inertial currents. For the stratified case, near-inertial internal waves are generated at land boundaries and propagate offshore with increasing frequencies, which induce tilting of velocity contours in the thermocline. The inertial oscillation is uniform across the whole basin, except near the coastal boundaries (~20 km) where it quickly declines to zero. This boundary effect is related to great enhancement of nonlinear terms, especially the vertical nonlinear term ($w\partial \mathbf{u} / \partial z$). With inclusion of near-inertial internal waves, the total near-inertial energy has a slight change, with occurrence of a small peak at ~50 km, which is similar to previous researches. We conclude that, for this distribution of near-inertial energy, the boundary effect for inertial oscillations is primary, and the near-inertial internal wave plays a secondary role. Homogeneous cases with various water depths (50 m, 40 m, 30 m, 20 m) are also simulated. It is found near-inertial energy monotonously declines with decreasing water depth, because more energy of initial wind-driven currents is transferred to seiches formed by barotropic waves. For the case of 20 m, the seiches energy even slightly overpasses the near-inertial energy. We suppose this is an important reason why near-inertial motions are weak and hardly observed in coastal regions.

Keywords: inertial oscillations, near-inertial internal waves, near-inertial energy

1. Introduction

Near-inertial motion has been observed and reported in many seas (e.g. Alford et al., 2016; Webster, 1968). It is mainly generated by changing winds at the sea surface (Pollard and Millard, 1970; Chen et al., 2015b). The passage of a cyclone or a front can induce very strong near-inertial motions(D'Asaro, 1985), which can last for 1-2 weeks and reach a maximum velocity magnitude of 0.5-1.0 m/s (Chen et al., 2015a; Zheng et al., 2006; Sun et al., 2011). In deep seas, the near-inertial internal wave propagates downwards to transfer energy to depth (Leaman and Sanford, 1975; Fu, 1981; Gill, 1984; Alford et al., 2012). The strong vertical shear of near-inertial currents may play an important role in inducing mixing across the thermocline (Price, 1981; Burchard and Rippeth, 2009).

In shelf seas, near-inertial motions exhibit a two-layer structure, with an opposite phase between currents in the surface and lower layers (Malone, 1968; Millot and Crepon, 1981; MacKinnon and Gregg, 2005). By solving a two-layer analytic model using the Laplace transform, Pettigrew (1981) found this 'baroclinic' structure can be formed by inertial oscillations without inclusion of near-inertial internal waves. Due to similar vertical structure and frequencies, inertial oscillations and near-inertial internal waves are hardly separable, and could easily be mistakenly recognized as each other.

In shelf seas, the near-inertial energy increases gradually offshore, and reaches a maximum near the shelf break, found both in observations (Chen et al., 1996) and model simulations (Xing et al., 2004; Nicholls et al., 2012). Chen and Xie (1997) reproduced this cross-shelf variation both in linear and nonlinear simulations, and attribute it to large values of the cross-shelf gradient of surface elevation and the vertical gradient of Reynolds stress near the shelf break. By using the analytic model of Pettigrew (1981), Shearman (2005) argued that the cross-shelf variation is controlled by baroclinic waves which emanate from the coast to introduce nullifying effects on the near-inertial energy near shore. Kundu et al. (1983) found a coastal inhibition of near-inertial energy within the Rossby radius from the coast, which is attributed to the downward and offshore leakage of near-inertial energy near the coast. As many factors seems to have effects, the mechanism controlling the cross-shelf variation of near-inertial energy seems complicated.

In this paper, simple two-dimensional simulations are used to investigate some basic features of near-inertial motions. Cases with and without vertical stratification are simulated to examine properties and differences of inertial oscillations and near-inertial internal waves. The horizontal distribution of near-inertial energy is discussed in detail. Also cases with various water depths are simulated to investigate the dependence of near-inertial motions on the water depth.

2. Model Settings

The simulated region is a two-dimensional shallow rectangular basin (300 km × 60 m). Numerical simulations are done by the MIT general circulation model (MITgcm) (Marshall et al., 1997), which discretizes the primitive equations and can be designed to model a wide range of phenomena. There are 1500 grids in the horizontal (Δx =200 m) and 60 grids in vertical (Δz =1 m). The water depth is uniform, with east and west sides being land boundaries. The vertical and horizontal eddy viscosities are assumed constants as 5×10^{-4} m^2/s and 10 m^2/s, respectively. The Coriolis parameter is 5×10^{-5} s^{-1} (at a latitude of 20.11 °N). The bottom boundary is no-slip. The model is forced by a spatially uniform wind which is kept westward and increases from 0 to 0.73 N/m^2 (corresponding to a wind speed of 20 m/s) for the first three hours and then suddenly stops. The model runs for 200 hours in total, with a time step of 4 seconds. The first case is homogeneous, while the second one has a stratification of two-layer structure initially. For the stratified case, the temperature is 20℃ in the upper layer ($-30 \text{ m} < z < 0$), and 15℃ in the lower layer ($-60 \text{ m} < z < -30 \text{ m}$). The salinity is constant, so the density is determined by the temperature. Except stratification all settings of these two cases are the same.

3. Inertial oscillation

The first case is without the presence of vertical stratification. Thus near-inertial internal wave is absent, and the near-inertial motion is pure inertial oscillations.

3.1 Vertical structures

The model simulated velocities (Fig. 1) vary near the inertial period (34.9 hours). Spectra of velocities (not shown) indicate maximum peaks located exactly at the inertial period. The spectra of u also have a smaller peak at the frequency of the first mode seiche. As this simulation is two-dimensional, i.e., the gradient along *y*-axis is zero, the seiche has little energy in v which shows clearly regular variation at the inertial frequency.

In the vertical direction, currents display a two-layer structure, with their phase being opposite between surface and lower layers. They are maximum at the surface, and have a weaker maximum in the lower layer (~40 m), with a minimum at the depth of ~20 m. The velocity gradually diminishes to zero at the bottom due to the bottom friction. This is the typical vertical structure of shelf-sea inertial oscillations, which have been frequently observed (Shearman, 2005; MacKinnon and Gregg, 2005). In practice, this vertical distribution can be modified due to presence of other processes, such as the surface maximum being pushed down to the subsurface (e.g. Chen et al., 2013). Note that without stratification in this simulation the near-inertial internal wave is absent. However, this two-layer structure of inertial oscillations looks 'baroclinic', which makes it easy to be mistakenly attributed to the near-inertial internal wave (Pettigrew, 1981).

It is interesting that currents of non-baroclinic inertial oscillations reverse between the surface and lower layers. This is usually attributed to the presence of the coast, which requires the normal-to-coast transport to be zero, thus currents in upper and lower layers compensate each other (Millot and Crepon, 1981; Chen et al., 1996). However, it remains unclear how this vertical structure is established.

As the westward wind blows for first three hours, the initial inertial current is also westward and only exists in the very surface layer (Fig. 2). In the lower layer there is no movement initially. Thus a westward transport is produced, which generates a rise (in the west) and fall (in the east) of elevation near coastal boundaries. The elevation slope behaves in a form of barotropic wave which propagates offshore at a great speed (87 km/h). The current driven by the barotropic wave is eastward, and uniform vertically. Therefore, with arrival of the barotropic wave the westward current in the surface is reduced, and the movement in the lower layer commences (Fig. 2). After passage of the first two barotropic waves (originated from both sides), currents in the lower layer have reached a relatively great value, while currents in the surface layer have been largely decreased (Fig. 3a). Accordingly, the depth-integrated transport diminishes a lot. This is like a feedback between inertial currents and barotropic waves. If only the depth-integrated transport of currents exist, barotropic waves will be generated, which reduce the surface currents but increase the lower layer currents, thus reduces the current transport. It will end up with inertial currents in the surface and lower layers having opposite directions and comparable amplitudes. As seen from Fig. 1b, the typical vertical structure of inertial currents is established within the first inertial period.

3.2 Horizontal distributions of inertial energy

The inertial velocities are almost entirely the same across the basin (Fig. 4), except near the boundary. This indicates that inertial oscillations have a coherence scale of almost the basin width. This is because in our simulation the wind force is spatially uniform, and the bottom is flat. The inertial velocities in the lower layer have slightly more variation across the basin than those in the surface layer, because inertial velocities in the lower layer is correlated to propagation of barotropic waves as discussed in 3.1, while the surface inertial currents are driven by spatially uniform wind. In shelf sea regions, the wind forcing is usually coherent as the synoptic scale is much larger, however, the topography that is mostly not flat could generate barotropic waves at various places, and thus significantly decrease coherence of inertial currents in the lower layer.

The spectra of velocities in the inertial band are almost uniform except near the boundaries (Fig. 5), consistent with the velocities. Near the boundaries, the inertial energy declines gradually to zero from x=~20 km to the coast wall. The east side has slightly greater inertial energy and a bit wider boundary layer compared to the west side.

We calculate the nonlinear and inertial terms in the momentum equation and find that nonlinear terms are of relatively high values initially within 2 km away from the land boundary (Fig 6bc), where the inertial term is smaller (Fig 6a). For the time-averaged values (Fig 6d), the vertical nonlinear term is two times more than the horizontal nonlinear term. The inertial term drops sharply near the boundary, and rises gradually with the distance away from the boundary. At x> 15km, it keeps an almost constant value which is much greater than nonlinear terms. Thus it is concluded that the significant decrease of inertial oscillations near the boundary is due to influence of nonlinear terms, especially the vertical nonlinear term.

4. Near-inertial internal waves

In addition to inertial oscillations, near-inertial internal waves are usually generated along when the vertical stratification is present. However, due to their close frequencies inertial oscillations and near-inertial internal waves are difficult to be separated. Thus we run a second simulation with the presence of stratification to investigate differences that near-inertial internal waves introduce.

4.1 Temperature distributions

Fig. 7 shows the evolution of temperature profiles with time. One can see an internal wave packet is generated at the west coast, and then propagates offshore. The wave phase speed is around 1 km/h, consistent with the theoretical value computed using the stratification. Before arrival of internal waves, the temperature at mid-depth diffuses gradually due to vertical diffusion in the model. For a fixed position at x=20 km (Fig. 8), the temperature varies with the inertial period (34.9 hours) and the amplitude of fluctuation declines gradually with time. At x=60 km and x=100 km, the strength of internal waves is much reduced. And wave periods are shorter initially, followed by a gradually increase to the inertial period. At x=140 km, the internal wave becomes as weak as the background disturbance.

A spectral analysis of the temperature at mid-depth (z=-30 m) is shown in Fig. 9a. The strongest peak is at near the inertial frequency (0.69 cpd), but only confined to the region close to the boundary (x<40 km). In the region 20km<x<70km, the energy is also large at higher frequencies of 0.8-1.7 cpd. This generally agrees with properties of Poincaré waves. During a Rossby adjustment, the waves with higher frequencies propagate offshore at greater group speeds, thus for places further offshore the waves have higher frequencies (Millot and Crepon, 1981). While the wave with a frequency closest to the inertial frequency moves at the slowest group velocity, and it takes a relatively long time to propagate far offshore, thus it is mostly confined to near the boundary. By solving an idealized two-layer model equation, the response of Rossby adjustment can be expressed in form of Bessel functions (Millot and Crepon, 1981; Gill, 1982; Pettigrew, 1981), as in Fig. 9cd showing the spectra of mid-depth elevation. The difference from our case is obvious. The frequency of theoretical near-inertial waves increase gradually with the distance from the coast, while in our case this property is absent. And the theoretical inertial energy has a e-folding scale of almost the Rossby radius (54 km), while in our case the e-folding scale is much smaller (~15 km).

4.2 Velocity distributions

With presence of near-inertial internal waves, the contours of velocities near the thermocline tilt slightly (Fig. 10d), and indicates an upward propagation of phase, thus a downward energy flux. This can also be seen in vertical spirals of velocities (Figs. 10e and 10f). With only inertial oscillations, current vectors mostly point toward two opposite directions. Once the near-inertial wave is included, the current vectors gradually rotate clockwise with depth.

The spatial distribution of the near-inertial energy is also slightly changed compared to the case with only inertial oscillations (Fig. 11 and Fig. 5). It is also greatly reduced to zero in the boundary layer (0-20 km) like the case without stratification. But at ~50 km away from the boundary the inertial energy reaches a peak. Further away (>100 km) it becomes a constant. This spatial distribution of inertial energy is similar to that observed in shelf seas, with maximum near the shelf break (Chen et al., 1996; Shearman, 2005). In our case, the boundary layer effect which induces a sharp decrease to zero makes a major contribution, and near-inertial internal waves which bring a small peak further offshore make a secondary influence.

5. Dependence on the water depth

In coastal regions, near-inertial motions are rarely reported. It is speculated that the strong dissipation and bottoms friction in coastal region suppress the development of near-inertial motions. However, Chen (2014) found the water depth is also a sensitive factor, with significant reduction for the case with smaller water depth. Here we will run cases with different water depths and clarify why the near-inertial energy changes with water depth. Homogeneous cases with water depths of 50 m, 40 m, 30 m, 20 m are simulated. The vertical interval for all cases is 1 m. All the other parameters including viscosities are the same as the homogeneous case of 60 m.

For each case, the currents are band-pass filtered to obtain near-inertial currents. Then near-inertial kinetic energy can be calculated. As seen in Fig. 12, the near-inertial energy gradually declines with decreasing water depth. In this dynamics system, the other dominant process are the seiches induced by barotropic waves. As the elevation induced by seiches is anti-symmetric in such a basin, the potential energy is little. The kinetic energy of siehces can also be calculated by the band-pass filtered currents. We find the energy of seiches, by contrast, increases gradually with decreasing water depth. For the case of 60m, the near-inertial energy is much greater than the seiches energy. But for the case of 20 m, the energy of seiches has overpasses the near-inertial energy slightly. The sum energy of these two processes almost keeps constant with varying water depth. For a shallower water depth, the reduction of near-inertial energy equals the increase of seiches energy. The initial current is wind-driven and only distributes in the surface layer. The unbalanced across-shelf flow generates elevation near the land boundary which propagates offshore as barotropic waves and form seiches. Part of the energy goes to form inertial oscillations. For a shallower water depth, the elevation is enlarged, and more energy is transferred to form seiches, thus with weakened near-inertial motions. Therefore, in coastal regions with water depth less than 30m, the near-inertial motion is weak, due to the suppressing of barotropic waves.

As seen in Section 3.1, inertial oscillations behave in a two-layer structure, with currents in the upper layer in opposite phase with those of lower layer. In terms of kinetic energy, for the case of 60 m (Fig. 13), the near-inertial motion is maximized in the very surface, minimized near the depth of 20 m, and then gradually increases with depth to form a much smaller peak at 40 m. Near the bottom, the near-inertial energy gradually reduces to zero due to bottom friction. When we set the bottom boundary condition from nonslip to slip, such a boundary structure vanishes, and near-inertial energy become constant in the lower layer. For other cases of 20 m and 40 m, their vertical profile are almost the same as the 60m case. The minimum positions are all located at 1/3 of the water depth. This implies the vertical distribution of near-inertial energy is independent of water depth. Note that in our cases, the vertical viscosity is set as a constant value. In practice, the viscosity in thermocline is usually significantly reduced, thus the minimum position of near-inertial energy is located just below the mixed layer.

6. Summary and discussion

Idealized simple two-dimensional (x-z) simulations are conducted to examine the response of a shallow closed basin to a wind pulse. The first case is homogeneous, in which properties the near-inertial motion is pure inertial oscillations. It has a two-layer structure, with currents in the surface and lower layers being opposite in phase, which has been reported frequently in shelf seas. We find that the inertial current is confined in the surface layer initially. The induced depth-integrated transport generates barotropic waves near boundaries which propagates quickly offshore. The flow driven by the barotropic wave is independent of depth and opposite to the surface flow. Thus the surface flow is reduced but the flow in the lower layer is increased, as a result the transport diminishes. This feedback between barotropic waves and currents continues and ends up with the depth-integrated transport vanishes, i.e., inertial currents in upper and low layers having opposite phases and comparable amplitudes. In our simulation, within just one inertial period the typical structure of inertial currents has been established. By solving a two-layer analytic model using the Laplace transform, Pettigrew (1981) also found the vertical structure of opposite currents associated with inertial oscillations. He argued that the arrival of a barotropic wave for a fixed location cancels half of the inertial oscillation in the surface layer, and initiates an equal and opposite oscillation in the lower layer. Our simulations further demonstrate the role of barotropic waves in forming this feature, and shows some more realistic details during this process.

The second case is set up with idealized two-layer stratification, thus near-inertial internal waves are generated. For a fixed position, velocity contours show clear obvious tiltings near the thermocline, and velocity vectors display clearly anti-cyclonic spirals with depth. These could be useful clues to examine occurrence of near-inertial internal waves. Near the land boundary the vertical elevation generates fluctuations of thermocline that propagate offshore. The energy of near-inertial internal waves is confined to near the land boundary (x< 40 km). At positions further offshore, the waves have higher frequencies. This is generally consistent with properties of Rossby adjustment process. However, our simulated result also shows evident discrepancies from theoretical values obtained in classic solutions of Rossby adjustment problem.

The inertial oscillation has a very large coherent scale of almost the basin scale (600 km). It is uniform in both amplitude and phase across the basin, except near the boundary (~20 km offshore). The energy of inertial oscillations declines gradually to zero from x=20 km to the coast. This boundary effect is attributed to influence of nonlinear terms, especially the vertical term ($w\partial\mathbf{u}/\partial z$), which are greatly enhanced near the boundary, and overweighs the inertial term ($f\mathbf{u}$). When near-inertial internal waves are produced in the stratified case, the distribution of total near-inertial energy is modified slightly near the boundary. A small peak appears at ~ 50 km offshore. This is similar to the cross-shelf distribution of near-inertial energy observed in shelf seas (Chen et al., 1996; Shearman, 2005). This energy distribution has been attributed to different reasons, such as downward and offshore leakage of near-inertial energy near the coast (Kundu et al., 1983), the variation of elevation and Reynolds stress terms associated with the topography (Chen and Xie, 1997) and the influence of the baroclinic wave (Shearman, 2005; Nicholls et al., 2012). In our simulations, this horizontal distribution of near-inertial energy is primarily controlled by the boundary effect on inertial oscillations, and the near-inertial internal wave makes a secondary effect.

Homogeneous cases with various water depths (50 m, 40 m, 30 m, 20 m and 10 m) are also simulated. The inertial energy is reduced with decreasing water depth, while the energy of seiches, by contrast, increases for the shallower case. For the case of 10 m, the seiches energy has slightly overpassed the inertial energy. It is interesting that the reduction of inertial energy just equals the increase of seiches energy, which implies more energy of initial wind-driven currents is transferred to the seiches for the shallower cases, and thus less energy goes to the inertial process. This is probably an important reason why near-inertial motions is weak and rarely reported in shallow coastal regions.

Acknowledgements

We are very appreciated for comments from John Huthnance. This study is supported by the National Basic Research Program of China (2014CB745002, 2015CB954004), the Shenzhen government (201510150880, SZHY2014-B01-001), and the Natural Science Foundation of China (41576008, 41276006, U1405233, and 40976013). Shengli Chen is sponsored by the China Postdoctoral Science Foundation (2016M591159).

References

Alford, M. H., Cronin, M. F., and Klymak, J. M.: Annual Cycle and Depth Penetration of Wind-Generated Near-Inertial Internal Waves at Ocean Station Papa in the Northeast Pacific, Journal of Physical Oceanography, 42, 889-909, 10.1175/jpo-d-11-092.1, 2012.

Alford, M. H., MacKinnon, J. A., Simmons, H. L., and Nash, J. D.: Near-Inertial Internal Gravity Waves in the Ocean, Ann Rev Mar Sci, 8, 95-123, 10.1146/annurev-marine-010814-015746, 2016.

Burchard, H., and Rippeth, T. P.: Generation of Bulk Shear Spikes in Shallow Stratified Tidal Seas, Journal of Physical Oceanography, 39, 969-985, 10.1175/2008jpo4074.1, 2009.

Chen, C., and Xie, L.: A numerical study of wind-induced, near-inertial oscillations over the Texas-Louisiana shelf, Journal of Geophysical Research: Oceans, 102, 15583-15593, 10.1029/97jc00228, 1997.

Chen, C. S., Reid, R. O., and Nowlin, W. D.: Near-inertial oscillations over the Texas Louisiana shelf, J Geophys Res-Oceans, 101, 3509-3524, 10.1029/95jc03395, 1996.

Chen, C. S.: Study on Several Features of the Near-inertial Motion, PhD, Xiamen University, 107 pp., 2014.

Chen, G., Xue, H., Wang, D., and Xie, Q.: Observed near-inertial kinetic energy in the northwestern South China Sea, J Geophys Res-Oceans, 118, 4965-4977, 10.1002/jgrc.20371, 2013.

Chen, S., Hu, J., and Polton, J. A.: Features of near-inertial motions observed on the northern South China Sea shelf during the passage of two typhoons, Acta Oceanologica Sinica, 34, 38-43, 10.1007/s13131-015-0594-y, 2015a.

Chen, S., Polton, J. A., Hu, J., and Xing, J.: Local inertial oscillations in the surface ocean generated by time-varying winds, Ocean Dynamics, 65, 1633-1641, 10.1007/s10236-015-0899-6, 2015b.

D'Asaro, E. A.: The energy flux from the wind to near-inertial motions in the surface mixed layer, Journal of Physical Oceanography, 15, 1043-1059, 1985.

Fu, L. L.: Observations and models of inertial waves in the deep ocean, Reviews of Geophysics, 19, 141-170, 10.1029/RG019i001p00141, 1981.

Gill, A. E.: Atmosphere-ocean dynamics, Academic Press, 662 pp., 1982.

Gill, A. E.: On the behavior of internal waves in the wakes of storms, Journal of Physical Oceanography,

14, 1129-1151, 10.1175/1520-0485(1984)014<1129:otboiw>2.0.co;2, 1984.
Kundu, P. K., Chao, S. Y., and McCreary, J. P.: Transient coastal currents and inertio-gravity waves, Deep-Sea Research Part a-Oceanographic Research Papers, 30, 1059-1082, 10.1016/0198-0149(83)90061-4, 1983.
Leaman, K. D., and Sanford, T. B.: Vertical energy propagation of inertial waves: a vector spectral analysis of velocity profiles, Journal of Geophysical Research, 80, 1975-1978, 1975.
MacKinnon, J. A., and Gregg, M. C.: Near-inertial waves on the New England shelf: The role of evolving stratification, turbulent dissipation, and bottom drag, Journal of Physical Oceanography, 35, 2408-2424, 10.1175/jpo2822.1, 2005.
Malone, F. D.: An analysis of current measurements in Lake Michigan, Journal of Geophysical Research, 73, 7065-&, 10.1029/JB073i022p07065, 1968.
Marshall, J., Adcroft, A., Hill, C., Perelman, L., and Heisey, C.: A finite-volume, incompressible Navier Stokes model for studies of the ocean on parallel computers, Journal of Geophysical Research: Oceans, 102, 5753-5766, 10.1029/96jc02775, 1997.
Millot, C., and Crepon, M.: Inertial oscillations on the continental-shelf of the Gulf of Lions - observations and theory, Journal of Physical Oceanography, 11, 639-657, 10.1175/1520-0485(1981)011<0639:iootcs>2.0.co;2, 1981.
Nicholls, J. F., Toumi, R., and Budgell, W. P.: Inertial currents in the Caspian Sea, Geophysical Research Letters, 39, 10.1029/2012gl052989, 2012.
Pettigrew, N. R.: The dynamics and kinematics of the coastal boundary layer off Long Island, 1981.
Pollard, R. T., and Millard, R. C.: Comparison between ovserved and simulated wind-generated inertial oscillations, Deep Sea Research, 813-821, 1970.
Price, J. F.: Upper ocean response to a hurricane, Journal of Physical Oceanography, 11, 153-175, 10.1175/1520-0485(1981)011<0153:uortah>2.0.co;2, 1981.
Shearman, R. K.: Observations of near-inertial current variability on the New England shelf, Journal of Geophysical Research, 110, 10.1029/2004jc002341, 2005.
Sun, Z., Hu, J., Zheng, Q., and Li, C.: Strong near-inertial oscillations in geostrophic shear in the northern South China Sea, Journal of Oceanography, 67, 377-384, 10.1007/s10872-011-0038-z, 2011.
Webster, F.: Observation of inertial period motions in the deep sea, Reviews of Geophysics, 6, 473-490, 1968.
Xing, J. X., Davies, A. M., and Fraunie, P.: Model studies of near-inertial motion on the continental shelf off northeast Spain: A three-dimensional two-dimensional one-dimensional model comparison study, J Geophys Res-Oceans, 109, 10.1029/2003jc001822, 2004.
Zheng, Q., Lai, R. J., and Huang, N. E.: Observation of ocean current response to 1998 Hurricane Georges in the Gulf of Mexico, Acta Oceanol. Sin., 25, 1-14, 2006.

Figures

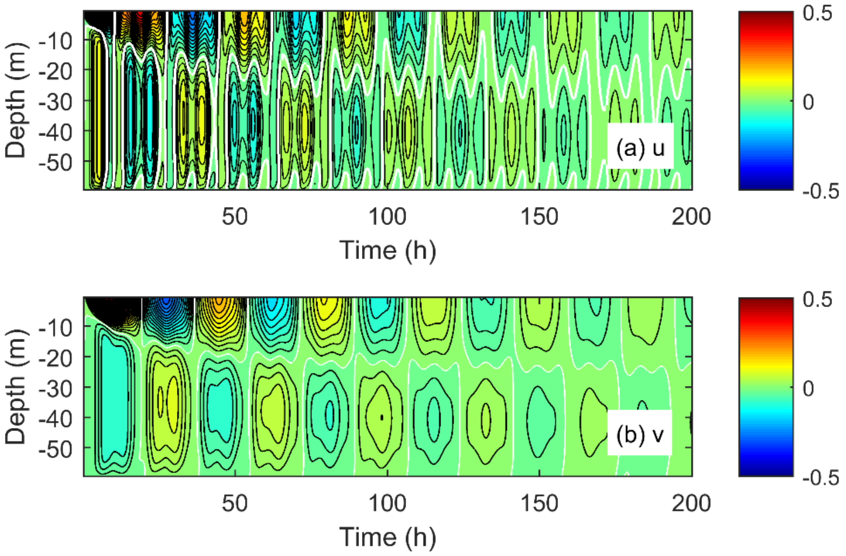

Fig. 1 Velocities (u and v, m/s) at x=70 km. The white lines denote the value of zero. The contour interval is 0.02 m/s for both panels.

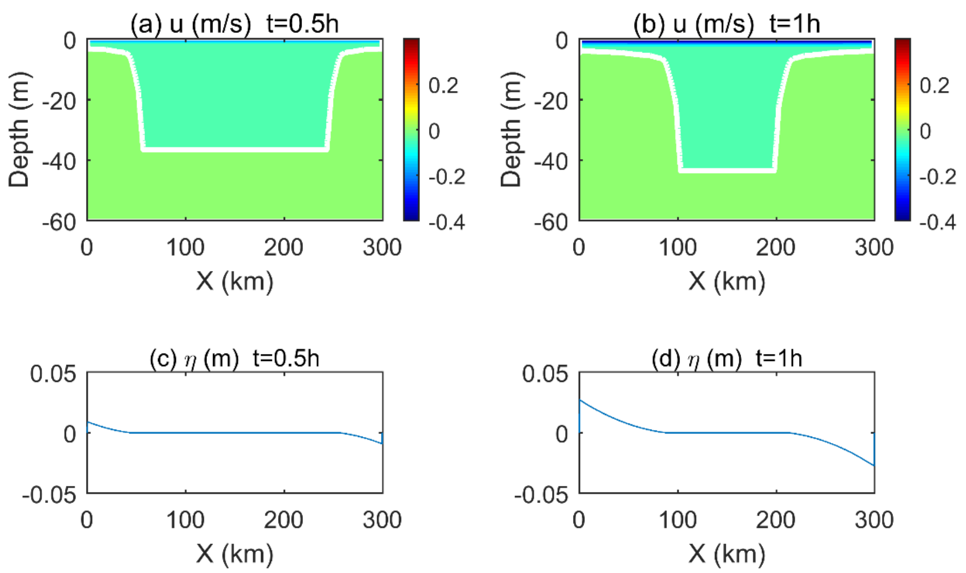

Fig. 2 Snapshots of eastward velocity and elevation (η) at t=0.5 and 1 hour. The white lines represent the value of zero.

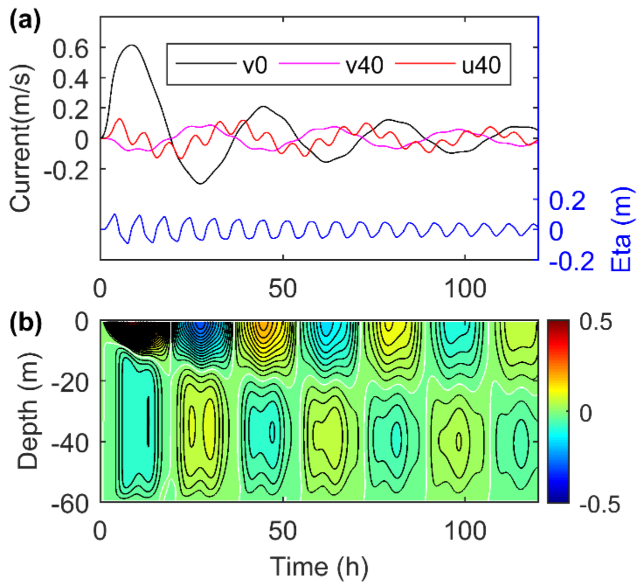

Fig. 3 (a) Time series of velocities and elevation at x=100 km. ‘v0’ and ‘v40’ mean the northward velocity (v) at depths of 0 m and 40 m, and ‘u40’ is the eastward velocity (u) at 40 m. (b) Contours of v at x=100 km. The white lines denote the value of zero, and the contour interval is 0.02 m/s.

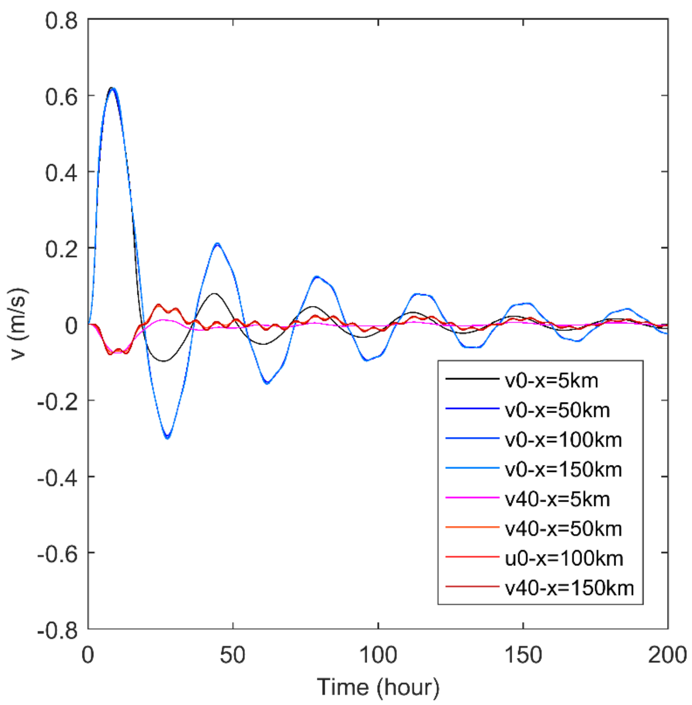

Fig. 4 Time series of the northward velocity (v) at different depths and positions. ‘v0’ and ‘v40’ mean v at depths of 0 m and 40 m.

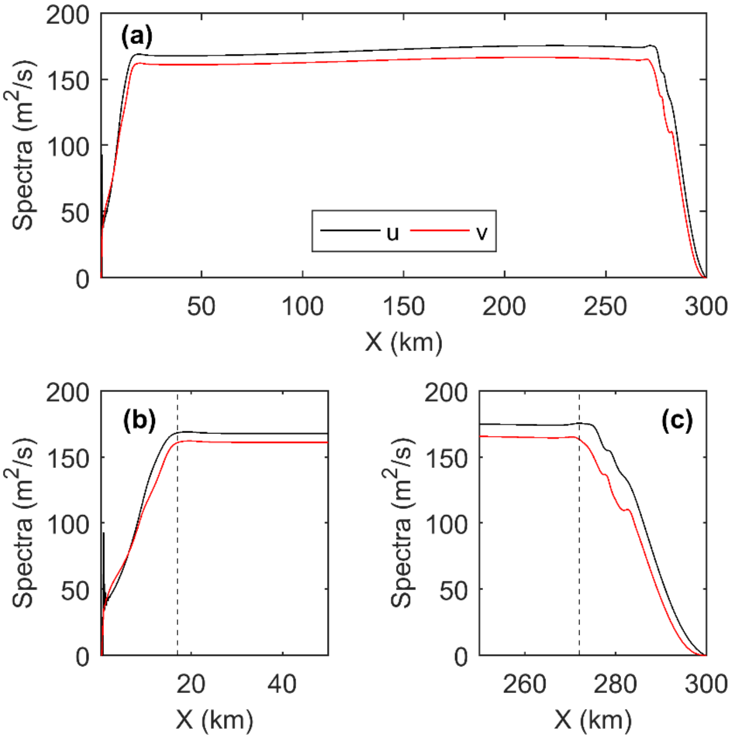

Fig. 5 Spatial variation of power spectra of velocities in near-inertial band for the homogeneous case. (b) and (c) display detailed values near boundaries.

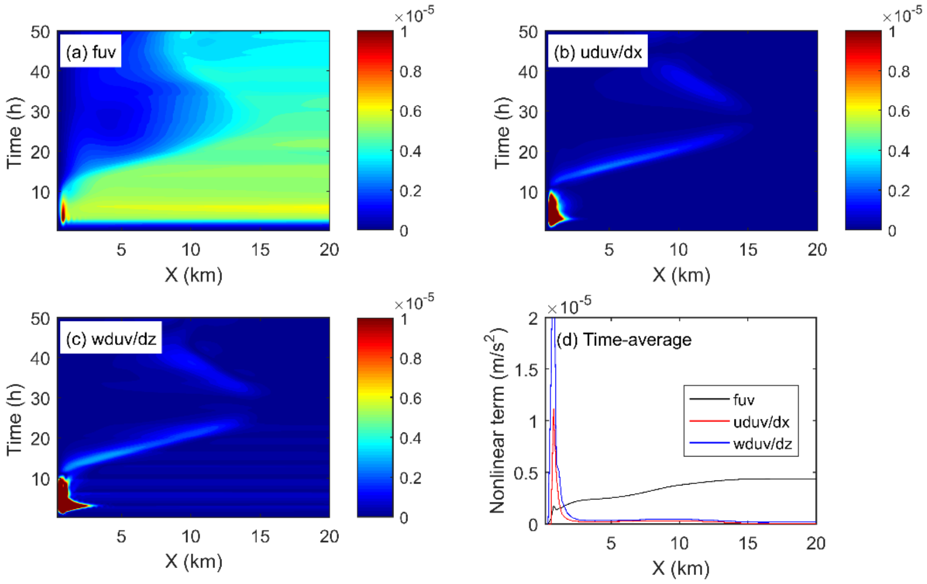

Fig 6. Variation of depth-mean inertial and nonlinear terms (m/s^2). The inertial term (a) is calculated as

$\left|f(u+iv)\right|$, the horizontal nonlinear term (b) is $\left|u\left(\partial u/\partial x+i\partial v/\partial x\right)\right|$, and the vertical nonlinear term (c) is $\left|w\left(\partial u/\partial z+i\partial v/\partial z\right)\right|$. (d) Time averaged value for the first 50 hours.

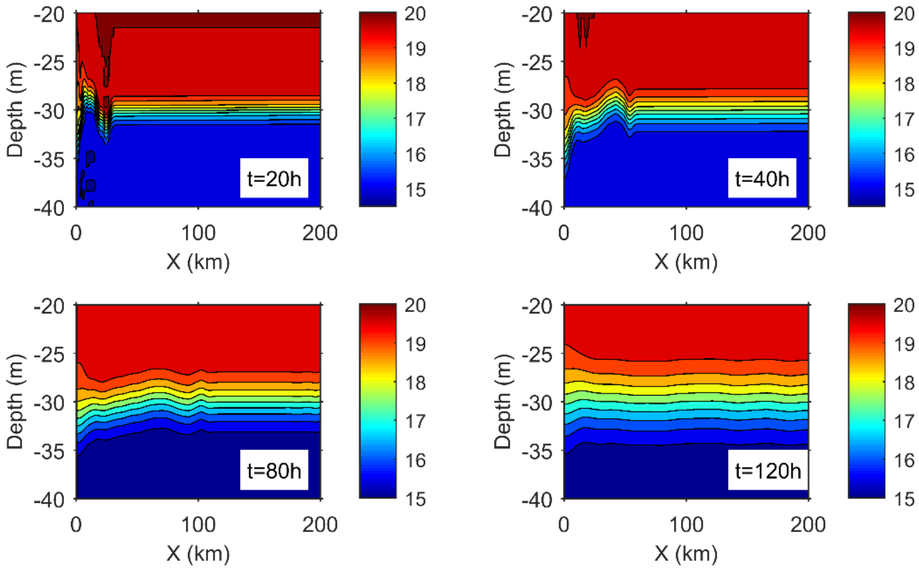

Fig. 7 Snapshots of temperature profiles at t=20h, 40h, 80h and 120h. The contour interval is 0.5 ℃.

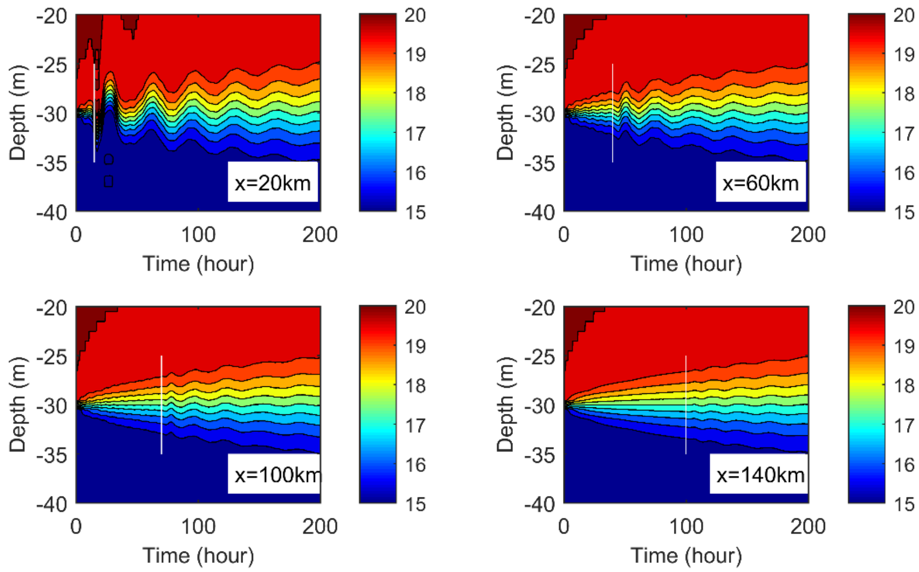

Fig. 8 Time series of temperature at x=20, 60, 100 and 140 km. White lines denote arrival of internal waves. The contour interval is 0.5 ℃.

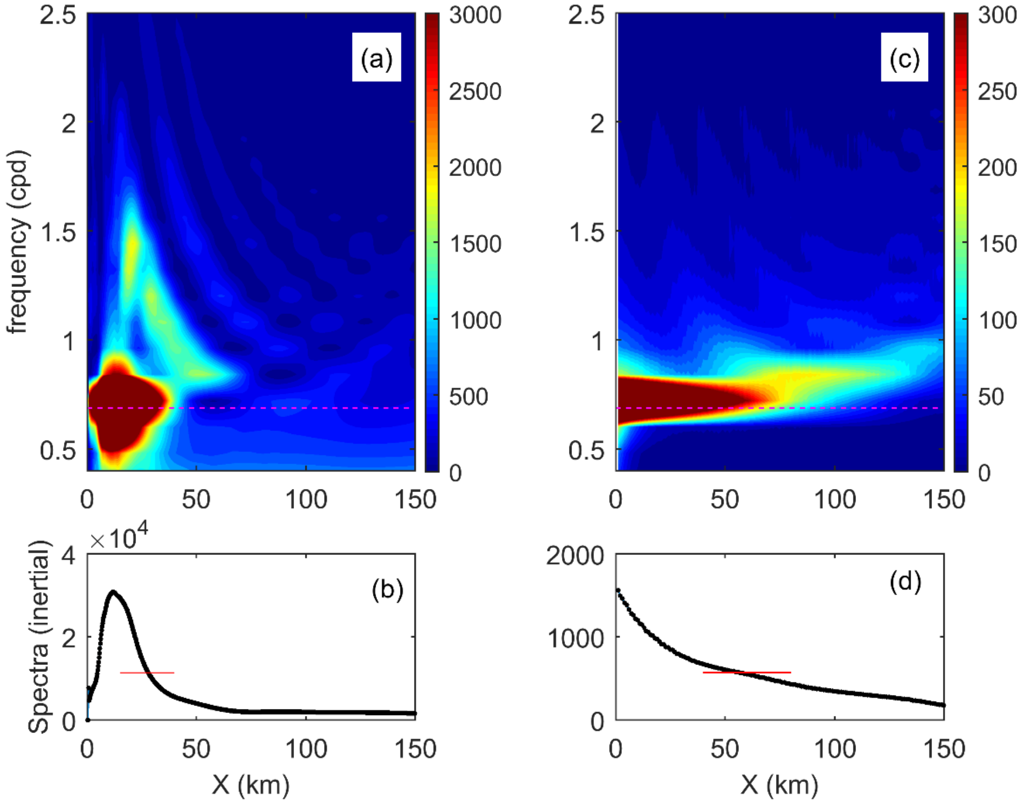

Fig. 9 (a) Spectra of the temperature at the mid-depth (z=-30 m). The pink dash line represents the inertial frequency, and the white line is the first mode seiche frequency. (b) Sum of spectra in inertial band with a red line denoting the e-folding value of the peak. (c) Theoretical spectra of mid-depth elevation calculated from the solution in the form of a Bessel function as in Eq. 3.16 of Pettigrew (1981). (d) Same as (b) but for theoretical spectra.

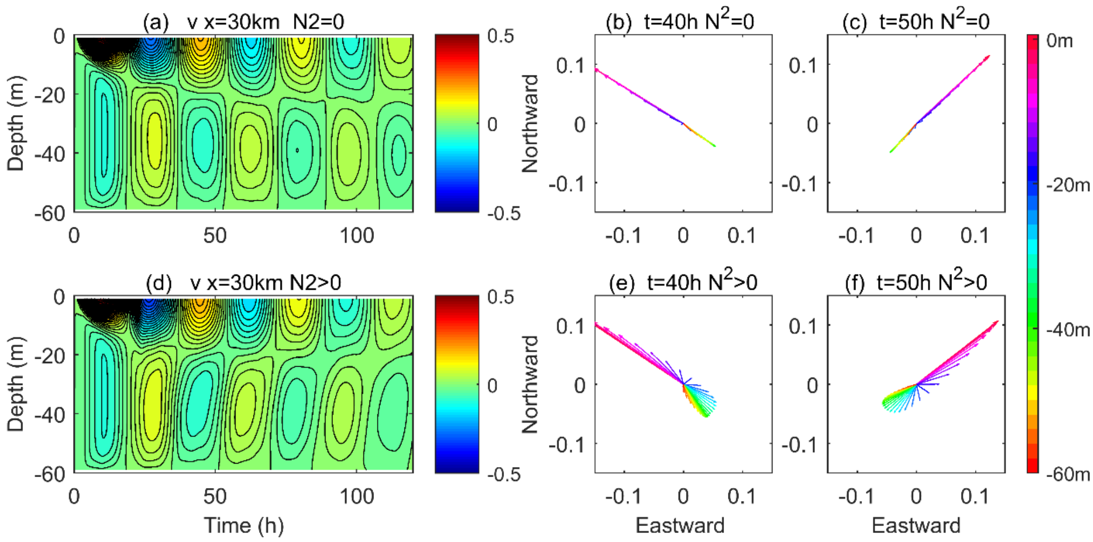

Fig. 10 Distribution of near-inertial currents (v, m/s) and current spirals for the cases without (a, b, c) and with (d, e, f) stratification at x=30 km. The near-inertial currents are obtained by applying a band-pass filter. The contour interval is 0.02 m/s.

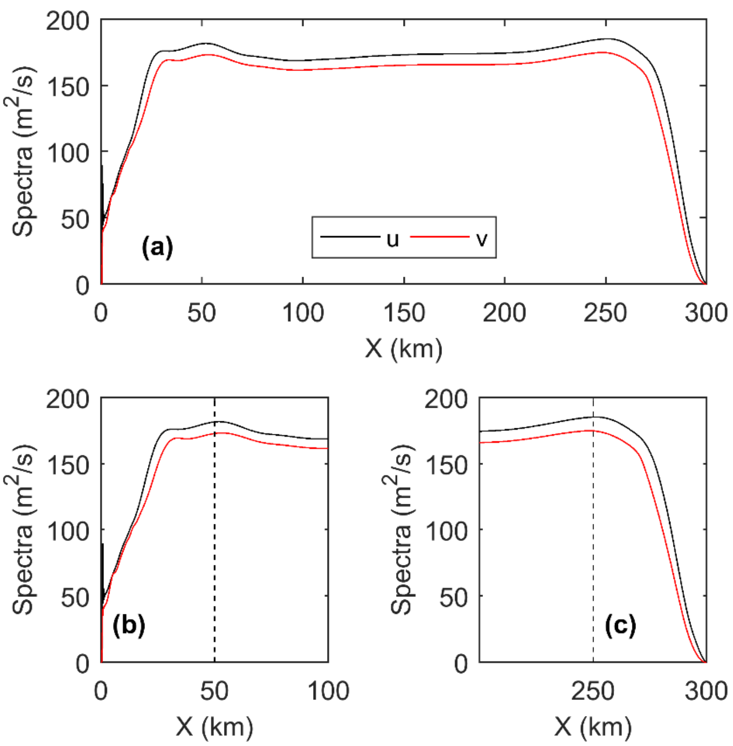

Fig. 11 Spatial variation of spectra of velocities in near-inertial band for the stratified case. (b) and (c) display detailed values near boundaries.

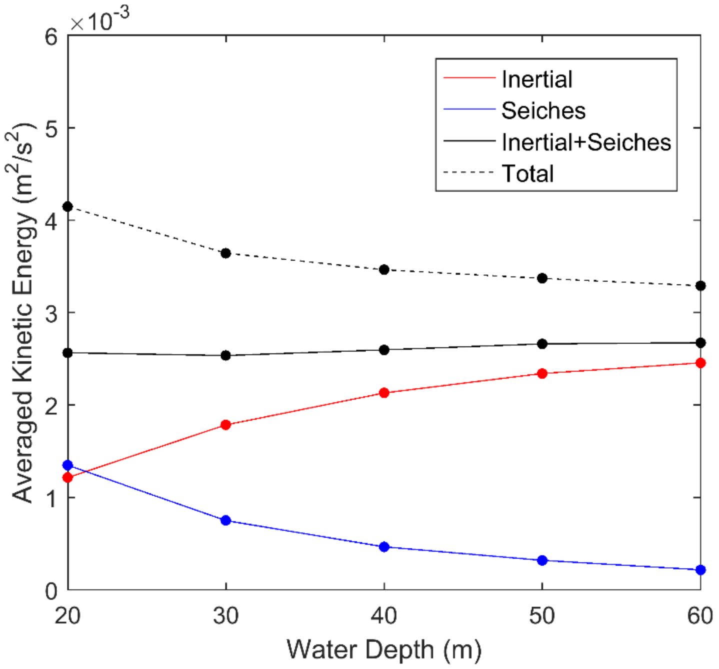

Fig. 12 The kinetic energy of near-inertial motions and seiches for different water depths. For each case, the currents are ban-pass filtered to get currents for each type of motions which are then averaged over time and integrated over space to obtain a final value.

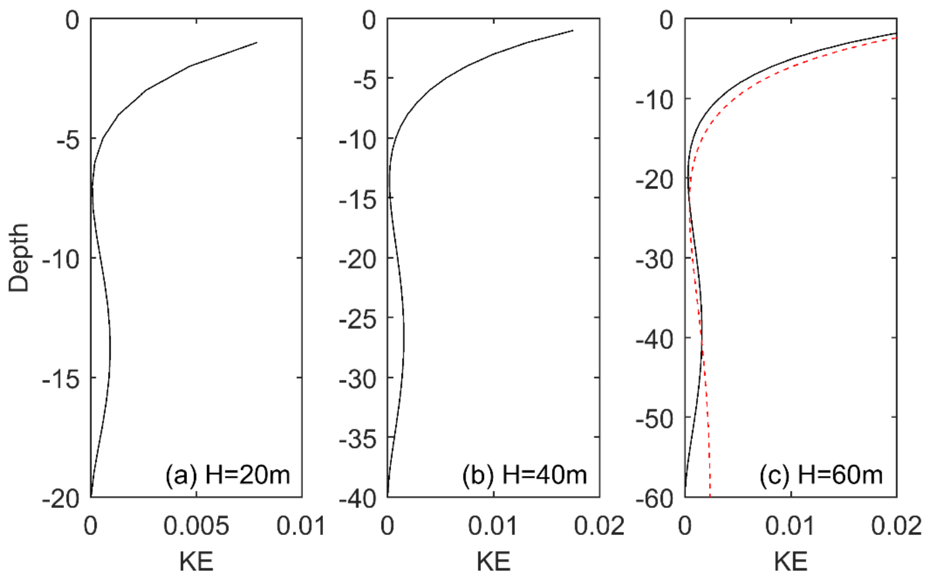

Fig. 13 Vertical profile of averaged inertial kinetic energy for the homogeneous cases with water depths of 20 m, 40 m and 60 m. The red dash line in (c) denotes the slip case.